On the role of a large shallow lake (Lake St. Clair, USA-Canada) in modulating phosphorus loads to Lake Erie

Serghei A. Bocaniov[1, 2,*], Philippe Van Cappellen[1], and Donald Scavia[3]

[1] Ecohydrology Research Group, Water Institute and Global Water Futures Program, University of Waterloo, Waterloo, ON, Canada.

[2] Graham Sustainability Institute, University of Michigan, Ann Arbor, Michigan, USA.

[3] School for Environment and Sustainability, University of Michigan, Ann Arbor, Michigan, USA.

* Corresponding author: sbocaniov@uwaterloo.ca serghei.bocaniov@gmail.com

This is the author manuscript accepted for publication and has undergone full peer review but has not been through the copyediting, typesetting, pagination and proofreading process, which may lead to differences between this version and the Version of Record. Please cite this article as doi: 10.1029/2019WR025019

Abstract

It is often assumed that large shallow water bodies are net sediment non-depositional annually, and that if they have nutrient loads from multiple sources, those loads are quickly homogenized before exiting the water bodies. Where this is not the case, it impacts understanding and predicting consequences of nutrient load reductions, both for the water body and for those downstream of it. We applied a three-dimensional ecological model to a large shallow lake, Lake St. Clair (US/Canada), to quantify the total and dissolved reactive phosphorus (TP and DRP) transport and retention, and construct tributary-specific relationships between phosphorus load to the lake and the amount of phosphorus that leaves the lake for the three major tributaries. Lake St. Clair is situated between the St. Clair and Detroit rivers, the latter enters Lake Erie. Efforts to reduce Lake Erie's re-eutrophication requires an understanding of nutrient transport and retention in each of its sub-watersheds including those that feed indirectly via Lake St. Clair. We found that over the simulation period, the lake retained a significant portion of TP (17%) and DRP (35%) load, and that TP and DRP retention was spatially variable and largely controlled by a combination of lake depth, resuspension, and plankton uptake. Compared to the Clinton and Sydenham rivers, the Thames River contributed a larger proportion of its load to the lake's outflow. However, because the lake's load is dominated by the St. Clair River, 40% reductions of nutrients from those sub-watersheds will result in less than a 5% reduction in the load to Lake Erie.

1. Introduction

While impacts of harmful algal blooms (HABs) and hypoxia were once reduced significantly in the Laurentian Great Lakes (Great Lakes afterwards), they have resurfaced, particularly in Lake Erie (Scavia et al., 2014). Under the 1978 binational Great Lakes Water Quality Agreement (GLWQA) (IJC, 1978), reductions in point sources of phosphorus (P) loads resulted in a 50% reduction in total P (TP) loading, with associated improvements in water quality and fisheries (Charlton et al., 1993; Ludsin et al., 2001). However, with changes in the ecology, climate, and the now dominant nonpoint P sources, Lake Erie's HAB and hypoxia extent and duration increased dramatically since the mid-1990s (Bridgeman et al., 2013; Scavia et al., 2014). The hypoxic area is now often comparable to the 1970s, with a new record size set in 2012 (Zhou et al., 2015) reaching a maximum daily extent of 11,600 km^2 (Karatayev et al., 2018), and toxic *Microcystis* blooms set records in 2011 (Michalak et al., 2013) and 2015, and the 2014 bloom led to a "do not drink" advisory for 500,000 people living in the Toledo, Ohio area (Ho and Michalak, 2015). In response to these changes, the U.S. and Canada revised Lake Erie's loading targets (GLWQA, 2016; IJC, 2012), based largely on science input from a multi-model effort (Scavia *et al*., 2016) and a public review process. The new targets call for reducing annual and spring (March-July) P loads to Lake Erie by 40 percent from their 2008 levels for west and central basins, while those for the east basin are still being developed and will be finalized in 2020. The task ahead is to develop and implement Domestic Action Plans (IJC, 2017) that achieve that reduction, primarily from the now dominant and harder to treat nonpoint sources.

The plans will undoubtedly address loads from all sources, but because the Detroit and Maumee rivers contribute 41% and 48% of the total P (TP) load and 59% and 31% of the

dissolved reactive P (DRP), respectively (Maccoux et al., 2016; Scavia et al., 2016, 2019), they will likely get special attention. Several efforts are in place to assess the relative contributions of, and potential controls of, P loads from the Maumee River watershed (e.g., Scavia et al., 2017; Muenich et al., 2016; Kalcic et al., 2016). Similar efforts are in place for the binational watersheds of the connecting channel between Lake Huron and Lake Erie (Scavia et al., 2019; Hu et al., 2018; Bocaniov and Scavia, 2018; Dagnew et al., 2019), but unlike the Maumee watershed, much of the connecting channel P loads do not flow directly into Lake Erie. Much of it must pass through the relatively large Lake St. Clair (Fig. 1a) that has its own sizable watershed consisting of both highly urbanized areas (e.g. Detroit, Windsor, London) and watersheds (e.g. Clinton River basin), as well as intensive agriculture in the Thames and Sydenham river basins.

The average annual relative phosphorus loads to Lake St. Clair for 2013-2015 are 71.5%, 4.8%, 12.1%, and 5.4% from the connecting channel (St. Clair River) and the three major tributaries, Clinton, Thames, and Sydenham rivers, respectively (Scavia et al., 2019). Because these are substantial inputs to the overall system, and because Scavia et al. (2019) estimate that Lake St. Clair retains, on average, 20% of its TP inputs, it is important to understand how P load reductions from individual tributaries to Lake St. Clair will correspond to the reduction in load to Lake Erie via the Detroit River.

In conducting this analysis, we show that large shallow lakes that are often considered well mixed cannot always be treated as homogeneous with respect to their individual tributary loads. This is because TP retention is a delicate balance between settling and resuspension, which are both in turn influenced by how winds, waves, water levels, lake-wide circulation pattern, and currents modulate tributary loads from different spatial locations. Here, we used a

previously calibrated and validated ecological model of Lake St. Clair (Bocaniov and Scavia, 2018; Figure SF-1) to show that this shallow polymictic (vertically well-mixed) lake is not spatially well mixed in relation to its external nutrient loads, explore and compare the biological and physical drivers of nutrient attenuation, and explore the sensitivity of nutrients leaving the lake to modifications in loads from each of its three major tributaries.

2. Methods

2.1 Study Site – Lake St. Clair is an integral part of the Laurentian Great Lakes system shared by Canada and the United States. However, in contrast to the Great Lakes proper, it is small (1114 km^2, 4.3 km^3) shallow (mean depth 3.9 m; Table 1; Fig 1b), with short theoretical water residence time (~9 days) and the largest ratio of watershed to lake surface area (13.8; =15400/1114) among all other lakes in the Great Lakes - Laurentian River Basin (Bocaniov and Scavia, 2018; Table 2). Its watershed is one of the most densely populated in the Great Lakes region, and this binational lake is an important source of drinking water, commercial and sport fishing, and other forms of recreation. Located in the connecting channel between Lakes Huron and Erie, the lake processes water from the upper Great Lakes (Superior, Michigan, Huron) via the St. Clair River, as well as from its proximate 15,400 km^2 watershed that is roughly 63% in Canada and 37% in the United States (Table 2). In addition to receiving P from the upper Great Lakes and the watersheds of the St. Clair River, it receives P from many direct tributaries, including significant loads from the Clinton, Thames, and Sydenham rivers, as well as point source discharges (Scavia et al., 2019). While the lake's theoretical flushing time is roughly 9 days, that flushing time (or water residence time) varies seasonally and, more significantly, spatially (Bocaniov and Scavia, 2018) such that during summer, water in the south-eastern part

of the lake flushes more slowly than water in the north-western part. This, in combination with different timing and magnitude of tributary loads, leads to spatial segmentation of primary production resulting in the northwest part of the lake being oligotrophic and southeast part mesotrophic (Bocaniov and Scavia, 2018).

2.2 River discharges – Characteristics of the sub-watersheds and daily flows (Tables 2-3) of the main inflow (St. Clair River), three major lake tributaries, and other smaller tributaries (Table 3; Fig. 1a) follow Bocaniov and Scavia (2018) and Scavia et al. (2019). Details of calculations and information on gauging stations can be found in Table S6 in Bocaniov and Scavia (2018) and Table S1 in Scavia et al. (2019). In brief, we downloaded data from the United States Geological Survey (USGS) National Water Information System (NWIS (U.S. Geological Survey, 2018)) for the US sites and from the Canada's HYDAT National Water Data Archive (HYDAT, 2018) for sites in Canada. For tributaries with multiple upstream flow gauges (e.g. the Sydenham River), we used area-weighted calculations to estimate flow at the downstream confluence. Similar to Scavia et al. (2019), flow values for tributaries without long-term flow gauges were estimated using area-weighted method based on values from nearby streams with flow gauges. To account for the most typical pattern in inter-annual hydrograph conditions in major lake tributaries (Thames, Sydenham, and Clinton rivers), as well as to preserve more typical/normal seasonal and inter-annual patterns in flow characteristics, rather than focus on a single year that may represent extreme conditions, we averaged daily values of river discharge over the past 17 years (2000 to 2016), so that a daily value for any given day was the average for that day of year over the 17-year study period. Because the St. Clair River discharge varies little from year to year, we used values from 2009 (Bocaniov and Scavia, 2018).

2.3 Meteorological, wave, water level and bottom currents data - For model simulations (2009) and our analysis of seasonal/inter-annual patterns in wind speeds and directions (2009 and 2010) we used meteorological observations collected at Detroit City Airport (Detroit, MI; 42.41°N, 83.01°W; anemometer height: 10 m above site elevation). The meteorological data were corrected to account for the open water conditions as in Bocaniov and Scavia (2018). For analysis of open water wave conditions (wave heights and periods), we used data collected during the seasonal buoy moorings (station #45147; Table ST-1) deployed in the middle of the lake (Fig. 1a) at 6 m depth and maintained by Environment and Climate Change Canada (ECCC). Water level data were analyzed based on observations at three gauging stations (Fig. 1a; Table ST-1): #9034052, # 9044049, and #11965. Water level data along with the lake bathymetry were used to calculate the representative lake volumes, mean and maximum depths, and allocation of bottom area into zones of similar depth with increments of about 1 m.

Field measured vertical profiles of lake currents, including both surface and bottom currents, can be useful in validating model hydrodynamics. Because bottom current observations were not available for 2009, we assumed data from ECCC's 2016 Doppler Current Profiler (ADCP) deployments were representative. Comparing these data with the results from other studies on the dynamics of the current velocities and flows in Lake St. Clair (Anderson et al., 2010; Anderson and Schwab, 2011) confirmed this assumption. The two ADCPs (stations A1-2; Fig. 1a; Table ST-1) were deployed in the south-eastern part of the lake from April 27 to November 3, and focused on near-bottom currents, their dynamics and characteristics. They were deployed at 0.5 m (A1) and 0.6 m (A2) above bottom and mounted on the bottom and configured as upward looking.

2.4 The Model - We used the three dimensional (3D) coupled hydrodynamic and ecological model previously applied to Lake St. Clair (Bocaniov and Scavia, 2018): The Estuary, Lake and Coastal Ocean Model (ELCOM) that drives the Computational Aquatic Ecosystem DYnamic Model (CAEDYM). ELCOM is a 3D hydrodynamic model that serves as the hydrodynamic driver for CAEDYM, a model capable of simulating a wide range of ecological processes and state variables (Hipsey, 2008; Hipsey and Hamilton, 2008). ELCOM-CAEDYM, with different levels of ecological complexity, has been used widely for large North American lakes, including Lakes Winnipeg, Ontario, Erie and St. Clair, for investigation of different aspects of nutrient and phytoplankton dynamics (e.g. Leon et al., 2011), relationship between transport time scales and nutrient losses (Bocaniov and Scavia, 2018), hypoxia (Bocaniov and Scavia, 2016; Bocaniov et al., 2016), the relative importance of meteorological forcing parameters (e.g. Liu et al., 2014; Bocaniov et al., 2014a), winter conditions (e.g. Oveisy et al., 2014), and the role of mussels in shaping temporal and spatial pattern of phytoplankton biomass (Bocaniov et al., 2014b) or interactions between hypoxia and spatial distribution of mussels (Karatayev et al., 2018).

For this application, we used the nutrient and phytoplankton components that simulate dynamics of phosphorus, nitrogen, and silica, and five functional groups of phytoplankton (e.g. Fig. SF-1; Table ST-2) and were described in earlier studies by Bocaniov et al. (2016) and Bocaniov and Scavia (2018). While this model does not simulate mussels and zooplankton as state variables, their grazing effects on phytoplankton are accounted for in phytoplankton loss rates. More detailed information on CAEDYM, and the specific details of its application to large lakes, is provided in Leon et al. (2011), Bocaniov *et al*. (2014b; 2016), and Bocaniov and Scavia (2018).

Lake St. Clair bathymetry, initial lake conditions, and meteorological drivers were assembled from the wide range of sources described in Bocaniov and Scavia (2018). The model was run with a computational grid resolution of 500 m × 500 m in horizontal (Fig. 1b) and 0.15 to 0.26 m in vertical dimension at a 5 min time step from March 1 through October 31. The model was calibrated and validated in previous applications (Bocaniov and Scavia, 2018).

2.5 Nutrient loading, retention, and tributary-specific nutrient response curves and retention times - Nutrient loads from the St. Clair River and three major tributaries (Thames, Sydenham and Clinton rivers) were calculated as in Scavia et al. (2019), using daily concentrations averaged over 2013 to 2015 which compared well with estimates from other studies (e.g. Burniston et al., 2018). For all other tributaries, which are minor in terms of flow and nutrient loads, the concentrations were kept as those as in 2009 (Bocaniov and Scavia, 2018).

Lake St. Clair TP and DRP retention for the March 1 through October 31 simulation period was estimated as the difference between the calibrated model's total input and total amount leaving the lake through the Detroit River, expressed as a percent of the total input. As such, the TP retention corresponds to the amount which has been removed from the system via settling, while the DRP retention corresponds to the amount converted from DRP to particulate organic P through biological uptake and incorporation into phytoplankton biomass, which may leave the lake via Detroit River and/or settle and be removed from the water column.

To explore the relative sensitivity of export from Lake St. Clair to changes in tributary loads, we developed tributary-specific response curves for the Clinton, Thames, and Sydenham rivers. For each tributary, one at a time, we additionally ran the model with a range of TP and DRP loads varied from the base load (Table 3) by 50%, 75%, 125% and 150% for each tributary

in question. The resulting loads leaving Lake St. Clair were plotted against the input loads. Because the load is dominated by the St. Clair River, we used the initial response curve to determine the intercept that was then subtracted from the loads and plotted again to provide a clearer comparison among slopes.

To estimate the lake residence times of river water from the St. Clair River and each of the three major tributaries, we used a model simulated conservative tracer in the river inflow and estimated the temporal dynamics of river water residence time as the difference between the accumulated amount of tracer that entered the lake and accumulated amount of tracer leaving the lake via the lake outflow.

Because previous studies of small shallow lakes emphasized that TP dynamics can be influenced by meteorological forcing and related physical processes, such as wind induced re-suspension (e.g. Hamilton & Mitchell, 1996; 1997), we explored if this was also true for larger lakes, such as Lake St. Clair. So, to explore the capacity of Lake St. Clair to modify nutrient transport and retention due to inter-annual variability in meteorological drivers, we estimated nutrient retention under different meteorological forcing scenarios, in addition to our basic run (Table 4), using observed meteorological conditions from different years, leaving all other conditions unchanged. To select the additional sets of meteorological conditions, we screened both the meteorological observations and satellite-derived lake surface temperatures between 1995 and 2014 and selected eight years to represent a wide range in wind speed and air temperature conditions (1995, 1996, 2003, 2005, 2008, 2010, 2012, and 2014; Table 4). For each set of meteorological conditions, we calculated retention of TP (R_{TP}) and DRP (R_{DRP}), and averaged over the entire simulation period air temperature ($\overline{AT}$) and wind speed ($\overline{WS}$). To explore

the relationships between nutrient retention and $\overline{AT}$ and $\overline{WS}$ we used bivariate or multivariate ordinary least squares regression models.

2.6. Segmenting the lake into wave-impact depth zones - The segmentation of the lake into zones was based on surface wave length and height. Season-averaged surface wave length (L_o) can be estimated from wave period (T) and for relatively deep water such as that at the location of buoy #45147 (depth 6 m) it can be calculated as in Masselink et al. (2014):

$$L_o = \frac{gT^2}{2\pi} \quad (1)$$

where g is the gravitational constant (9.807 m s^{-2}), and T is season-averaged wave period (s) estimated from measurements at buoy #45147 (Fig. 1a).

To partition the lake into two characteristic depth (D) zones based on the disturbance effect of surface waves on the lake bed we followed Masselink et al. (2014): (i) intermediate and shallow water where the lake bottom is affected by waves: $D/L_o < 0.5$; and, (ii) deep water where the lake bottom is affected by waves: $D/L_o > 0.5$.

2.7 Bottom Shear Stress – Sediment resuspension and particle entrainment into the water column occurs when the bottom shear stress becomes greater than the critical shear stress for the initiation of re-suspension (Van Rijn, 1993). Bottom shear stress (τ_{cw}) is caused by shear stress due to wind-driven surface waves (τ_w) and shear stress caused by the near-bed circulatory water currents (τ_c). The interaction between τ_w and τ_c , especially in deep aquatic systems, can be very complicated, and in cases when the wave and current boundary layers are turbulent, the combined wave-current bottom shear stress is highly nonlinear (Grant and Madsen, 1979; Glenn

and Grant, 1987). The bottom current shear stress due to currents (τ_c) can be calculated as in Hawley and Lesht (1992). However, previous studies in Lake St. Clair, other similar shallow lakes (e.g. Lake Balaton), and in shallow depths of deeper systems (e.g. Lake Michigan, etc.) have shown that τ_c is typically much smaller than τ_w and can be neglected (Luettich et al., 1990; Hawley and Lesht, 1992; Van Rijn, 1993; Hamilton and Mitchell, 1996). Therefore, τ_{cw} can be calculated from Equation 2:

$$\tau_{cw} = \tau_w \quad (2)$$

The bottom shear stress due to wind waves (τ_w) was calculated from wave height, period, and length, as in Hawley and Lesht (1992):

$$\tau_w = \frac{H \cdot \rho \cdot \nu^{0.5} \left(\frac{2\pi}{T}\right)^{1.5}}{2 \sinh\left(\frac{D2\pi}{L}\right)} \quad (3)$$

where τ_w is the bottom shear stress due to surface waves (N m^{-2}), H the significant wave height (m; observed), ρ the density of water (kg m^{-3}) and calculated as in Tanaka et al. (2001), υ the kinematic viscosity of water (cm^2 s^{-1}) and calculated as in Kestin et al. (1978), T the wave period (s; observed), D the local water depth (m; observed), and L the wave length calculated from T (m) and calculated as in Dean and Dalrymple (1984). To estimate the bottom shear stress due to surface waves we used the observed 2009 data on wave characteristics from ECCC buoy located in the middle of the lake (station 45147; Fig. 1a). To confirm that the bottom shear stress due to bottom currents by far smaller than τ_w and therefore can be neglected, we estimated τ_c by two independent methods. We used our model output for estimates of bottom currents in 2009 as well as the observed bottom currents based on ADCP measurements in 2016. In both cases, τ_c was smaller than τ_w by 12 to 15 times.

2.8 *Model validation* –We used a 3D coupled hydrodynamic and ecological model of Lake St. Clair that was calibrated and validated in previous applications to this lake (Bocaniov and Scavia, 2018). Here, we extend that validation work to include spatial and temporal dynamics of current velocities, and a larger number of physical and bio-chemical water quality parameters. The hydrodynamic and water budget component of the model was verified first for 2009 and 2010 temperatures and water level observations. The temperature verification included satellite-derived lake-wide observation of the daily mean surface water temperature, hourly surface water temperature measured at the location of station #45147 (Table ST-1; Fig. 1a), and discrete measurements of water temperature of lake outflow at the source of the Detroit River. Water level validation was based on the comparison of daily mean water levels predicted by the model and measured at the three water-level stations (Table ST-1; Fig. 1a). Because of the limited data available to verify the currents in 2009 and 2010, we compared the model predicted magnitude and temporal-spatial dynamics of near-bottom and surface current velocities to the available measurements in 2016 at two locations (stations A1-2; Table ST-1; Fig. 1a), and published data for 2008 (Anderson et al., 2010; Anderson and Schwab, 2011).

After being calibrated and validated, the model was rerun under 2009 conditions except with updated flows for three major tributaries (Thames, Sydenham, and Clinton rivers) that correspond to their multi-year average flow patterns with the necessary adjustments made to the outflow (Detroit River flow) to maintain the same water level in Lake St. Clair as in 2009. The adjustments made to the Detroit River flow were small and insignificant - within its natural river flow variability constituting less than one sixth of one standard deviation of its annual variability for the past 20 years (Detroit River flow for 1998-2017; mean ± SD: 5294.5 ± 426.4 $m^3 s^{-1}$)

2.9 *Lake-wide DRP budget* – While TP retention is directly related to the amount of the within-lake settled TP, the DRP retention is more complex, as it involves the transformations from dissolved to particulate form (e.g. algal uptake) and from dissolved organic form to dissolved inorganic form (e.g. microbial mineralization). Moreover, DRP retention does not distinguish between phytoplankton assimilated DRP that settles to the lake bottom and that which leaves the lake via its outflow (Detroit River). To better understand the dynamics of DRP retention, we constructed a DRP budget for the lake based on model output for the base case scenario for the entire run duration (244 days: March 1 to October 31, 2009). To do that, we used a model-derived whole-lake budget for DRP which included external inputs from all inflows and atmospheric load, export with lake outflow, internal loading from the sediments, and accounted for within-lake transformations such as incorporation into phytoplankton biomass and microbial mineralization of dissolved organic phosphorus.

3. Results

3.1. 3D Model validation.

Overall, the model was able to sufficiently represent the dynamic nature of physical and bio-chemical lake processes. It accurately reproduced observed temperatures and water levels over the simulation period (Table ST-3), and the simulated water quality parameters were in reasonable agreement with the field measurements (Table ST-3). Spatial and temporal variations in current velocities were also well reproduced (Table ST-4; Fig. SF-2).

3.2. Nutrient loads, retention, and response to reductions.

Estimates of flows, nutrient loads, and residence times for major tributary inputs – The St. Clair River was responsible for 97.1% of water load, and 78.1% and 71.9% of the TP and DRP loads, respectively (Table 3). The Thames, Sydenham, and Clinton rivers together accounted for roughly 2.1% of lake water load and 18.8% and 23.5% of the TP and DRP loads. All other tributaries were responsible for about 0.1% of the inflow and 1.3% and 2.8% of the TP and DRP loads, respectively. Over-lake precipitation and atmospheric load of phosphorus load accounted for about 0.7% lake water inflow and 1.7% and 1.8% of the TP and DRP loads, respectively.

Based on conservative tracers released with the St. Clair River and tributary inflows, the St. Clair River had the shortest water residence time (WRT) ranging from 3 to 7 days with a mean value of 5 days. WRTs for the tributaries were short in spring and longer in summer and fall. In spring, WRTs were 8, 11 and 11 days for Clinton, Sydenham, and Thames rivers, respectively. In summer and fall, they increased to 21, 35 and 39 days, respectively. The spatial and temporal distribution of the Thames river water mass shows that it tends to have a strong local effect (Fig. 2) in the vicinity of the Thames River mouth and along the south-east and south shores. The presence of Thames river in locations further offshore was generally small, with the largest values in March and April and then decreasing towards May and June and almost zero in July and following months. Water from the Sydenham River (not shown) generally moved along the north-western part of the lake but was more diluted with the lake water compared to the Thames. Clinton River water (Fig. 3) was diluted and mixed rapidly with the strong flow of the St. Clair River water. Depending on the winds, its waters can be advected into shallow Anchor Bay, and/or L'anse Creuse Bay (Fig.1a).

TP and DRP Retention (R_{TP}, R_{DRP}) and the relation to atmospheric forcing – Lake-scale retention during the simulation period (March 1 to October 31) for the base case (2009; Scenario B; Table 4) was 17.3% for TP (R_{TP}; Table 5) and 34.8% for DRP (R_{DRP}; Table 6). Over the range of meteorological conditions tested (Table 4), average retention (±SD) was 17.8 ±2.3% for R_{TP} (Table 5) and 34.8 ±1.2% (Table 6) for R_{DRP}. R_{TP} was larger during the years with relatively lower winds (Table 5).

Seasonally averaged wind speed ($\overline{WS}$) and air temperature ($\overline{AT}$) for each meteorological forcing scenario are summarized in Tables 5 and 6. $\overline{WS}$ was a better predictor than $\overline{AT}$ of R_{TP} and R_{DRP} (Table 7). There was a strong and statistically significant negative relationship between $\overline{WS}$ and R_{TP}. While $\overline{AT}$ alone was not a significant variable, it added significantly and positively to the variance already explained by $\overline{WS}$. R_{DRP} was also significantly and negatively related to $\overline{WS}$. Similar to with R_{TP}, $\overline{AT}$ alone was not a good predictor, but it added significantly to the amount of variance already explained by $\overline{WS}$. R_{DRP} and R_{TP} were strongly related and the former can be expressed as a constant value (172 MT) plus 13% of R_{TP} (Table 7, model 7).

Tributary-specific nutrient response curves – All TP and DRP load-response curves were linear (Fig. 4), indicating proportional changes in the nutrient load leaving the lake outflow through the Detroit River as a function of load reductions in the tributaries. For TP (Fig. 4a), the slopes for the Sydenham and Clinton rivers were similar (0.55 and 0.54, respectively) and lower than for the Thames river (0.65). For DRP (Fig. 4b), the Clinton river had a smaller slope (0.53) than for the Thames and Sydenham rivers (0.65 and 0.66, respectively). Consistent with the retention estimates, all slopes were less than 1, indicating that the reduction in total load to the Detroit River was smaller than the reduction of the nutrient load in any of the Lake St. Clair tributaries.

3.3. Drivers and controls of nutrient retention and load response.

To explore potential mechanisms controlling variation in time and space, among tributaries, and between TP and DRP of retention and response, we analyzed winds, waves, and currents in the context of water levels, bathymetry, and sediment deposition and resuspension.

Winds, waves, and near-bottom currents – Wind frequencies, speed, and directions at the Detroit City Airport meteorological station in 2009 (Figs. SF–3-5) and 2010 (Figs. SF–6-8) followed a seasonal cycle with some inter-annual variability. Winds were more frequent westerly (west and southwest, but also from the northwest) with some exceptions, such as during spring when winds were either blowing equally from all directions or more frequent from the north-east.

Observed wave periods were typically short with median and mean (±SD) values of 2 s and 2.44 ±0.56 s, respectively at buoy #45147 (April 20 to December 7, 2009). Wave heights were typically small (Fig. SF–9), with the most frequent observation (25.3%) being 0.1 m and waves exceeding 0.7 m occurred in less than 1.2% of the observation period. Excluding periods of calm, the median significant wave height was 0.30 m with a mean of 0.29 ±0.17 m. While stronger winds generated larger waves in spring and fall, their durations were short lived.

Near-bottom currents measured at stations A1 and A2 ranged from < 1 to about 15 and 24 cm s^{-1} during storms (Table ST–4, Figs. SF–10-13), but were typically small and for the depths closest to the bottom, the overall monthly means of 2.5 ±1.5 and 3.7 ±2.7 cm s^{-1} at stations A1 and A2, respectively.

Current- and wave-induced bottom shear stress - Estimated bottom shear stress due to wave action (τ_w) based on wave characteristics observed at ECCC wave buoy (station 45147; Fig. 1a) was largely dependent on local depth (Fig. 5). At shallow sites (e.g. 2-4 m; Fig. 5a-c) it frequently approached or exceeded the critical shear stress (τ_{crit} = 0.25 N m^{-2}). While at deeper (≥ 5 m) sites, it could exceed τ_{crit} during storms but was less than τ_{crit} for long periods of time (Fig. 5d-f). Because near-bottom currents were slow, calculated current-related bottom shear stress (τ_c), based on ADCPs measurements in 2016 conducted by ECCC (stations A1-2; Fig. 1a), was small (mean ±SD of 0.005 ±0.007 and 0.013 ±0.023 N m^{-2} for A1 and A2, respectively), typically an order of magnitude smaller than τ_w. Additional estimates of τ_c based on the model output for 2009 and for the same locations as stations A1 and A2 returned similar τ_c values as those based on the ADCP measurements in 2016.

Lake depth and wave disturbing effects − Our analysis of wave characteristics observed at buoy #45147 (Fig. 1a) suggest the lake bed can be characterized as two distinct zones: shallow and intermediate water zone where lake bed is affected by waves (≤ 4.9 m), and deep water zone where lake bed is unaffected by surface waves (depth 5 to 6.4 m) for most of the time. This deep water zone (≥ 5 m) was similar to those depths where the bottom shear stress tended not to exceed τ_{crit} for most of the time (e.g. Fig. 5d-f). Though lake is shallow (Fig. 1b; Table 1), there is a significant portion of the lake bottom area with the depth ≥ 5 m (Table 8) accounting for almost 30% of the entire lake area.

Spatial and temporal dynamics in DRP retention (R_{DRP}) – R_{DRP} had a clear temporal trend (Fig. SF-14a). It was lowest in spring (March and April) under the conditions of low phytoplankton

biomass, low water temperature, short photoperiod, lower short-wave radiation and high flushing rates. It increased to maximum values in June when water temperatures are warm, the photoperiod is longest, and the short wave radiation is at its annual maximum. In July to September, R_{DRP} stayed elevated due to warm water temperatures, relatively long photoperiod and high solar radiation, lower flushing times, and elevated standing biomass of phytoplankton. In October, with autumnal cooling, storms, and lower solar radiation, R_{DRP} became 3-5 times lower than summer rates.

R_{DRP} also had a spatial component. It was larger in areas with longer local water residence time (water age) where phytoplankton biomass can become high (Figs. 11 & 12 in Bocaniov and Scavia, 2018; see Fig. SF–15). Such zones are located in the eastern and south-eastern parts of the lake.

Model derived DRP budget and insights into lake-wide DRP retention - Our model results (Table ST–5; Fig. SF–16) indicated a downstream export of 182 MT of DRP incorporated in the fresh algal biomass (autochthonous production), indicating a within-lake net settling of 104 MT of DRP that had been incorporated in fresh algal biomass (autochthonous production). The amount of 182 MT is within the statistically-derived slope ± standard error (SE) of model 7 (172 ±14.5 MT; Table 7). The 10 MT DRP difference represents recycling of autochthonous source of DRP. The remaining amount of the mineralized DRP (69-10 = 59 MT) was incorporated in settled algal biomass. This suggests that the amount of externally derived DRP incorporated in the settled fresh algal biomass is 45 MT (104 – 59 = 45 MT) which constitutes about 13.5% of total TP retention (or the total amount of TP removed from the water column via

settling to the lake bottom). This model derived value is in good agreement with the statistically derived number (13% of TP retention; Table 7, model 7).

Our model results indicated that sediment flux of DRP was both from the sediments and into the sediments, but was of very low magnitude reflecting the well oxygenated conditions and pH values in the neutral range. Overall, the contribution of sediment flux of DRP to R_{DRP} was less than 1%. The algal uptake of allochthonous (external inputs) DRP was the most important form of phytoplankton uptake, making up about 79% of total uptake. The downstream export of inorganic DRP was 407 MT and was dominated by the allochthonous DRP (98%) because the autochthonous DRP was more efficiently recycled and retained within the system [86%; = (59/69)*100%; Fig. SF-16; Table ST-5] compared to lower retention efficiency of allochthonous DRP [36%; = (227/624)*100%].

4. Discussion

Phosphorus retention – In our numerical model, TP retention represents the amount of phosphorus removed, primarily by settling, while in the real world, TP can also be retained by incorporation in macrophytes. We showed that during March 1 to October 31, the lake was a net sink for phosphorus with an average TP retention under different observed meteorological forcing (Table 4) of about 18% (Table 5). This retention rate estimate is similar to the 1998-2016 average annual retention of 20% estimated with a TP mass balance based on measured loads into and out of the lake (Scavia et al., 2019), and the variability with meteorological conditions (Table 7) may explain the substantial inter-annual variability (4-34%) Scavia et al. (2019) reported. The small difference between our estimate and that of Scavia et al. (2019) may be

because our simulation period did not include ice-covered season when the lake surface is sheltered from the effects of surface wind stress and settling rates should dominate resuspension. Our model also did not include rooted aquatic macrophytes, which may attenuate the bottom shear stress and thus reduce the resuspension.

Scavia et al. (2019) concluded that the Lang et al. (1988) estimate of TP retention was underestimated because it was based on an estimated load from Lake Huron and the St. Clair River loads rather than direct measurements into Lake St. Clair, and they showed that those estimates of the Lake Huron loads are underestimates. They also suggested that the discrepancy could be because of the significant dreissenid mussel invasion in the late 1980s (Nalepa et al., 1996). Nalepa et al. (1991) estimated that the mussel-related retention of TP during between May and October was 134 MT, corresponding to about 8.6% of the external TP load during the same period. Lang et al. (1988) estimated macrophyte growth to be on the order of 219 MTA, or roughly 7% of TP loads. So, together these could account for a substantial portion of the retention. However, physical controls also appear important.

Wind-induced control of nutrient retention - While the lake is shallow, with extensive areas where resuspension rates may be comparable to settling rates, there are deeper zones (≥ 5 m; Table 8) where currents and waves (see Table ST–4 and Figs. SF–10-13; Fig. SF–9) are not sufficient to generate bottom shear stresses exceeding τ_{crit} (e.g. Fig. 5). In addition, our results show a strong relationship between TP retention and season averaged wind speed (Table 7; models 1 and 3) with wind and wind along with air temperature being able to explain 89% and 96% of the variation in TP retention, respectively. This is consistent with sediment entrainment and burial being a function of bottom shear stress (τ_{cw}), which in shallow systems is largely

depend on wind-driven surface waves (Van Rijn, 1993). This is consistent with the fact that more than 70% of the lake bottom is susceptible to waves (Table 8) and that in relatively shallow lakes the TP dynamics is largely controlled by wind-induced resuspension (e.g. Hamilton and Mitchell, 1996; 1997). We also showed a statistically significant negative relationship between DRP retention and average wind speed, though weaker than that for TP. Hamilton and Mitchell (1997) also found the relationships between DRP and wind-induced bottom shear stress to be considerably weaker than those for TP, and inconsistent across the seven shallow lakes they studied. The stronger relationship for TP is expected because, unlike DRP, particulate phosphorus is controlled primarily by the balance between settling and resuspension, with the latter driven by the wind-induced resuspension.

It is interesting to note that while wind has a negative effect on TP retention, air temperature has a positive effect. Warmer temperatures can increase settling and therefore burial and retention through its effect on bottom shear stress and settling via its effects on water density and viscosity (see Eq. 3), and by facilitating the transformation of DRP to TP via increased incorporation by phytoplankton.

The relationship between R_{DRP} and R_{TP} (Table 7, model 7) suggest that the former is a product of two components. One represents the relatively constant amount of DRP converted to algal biomass and exported via the lake outflow (~172 MT; intercept of model 7). Because this is constant across scenarios, it might suggest that algal production is limited more by flushing than by nutrients and/or light. The second component suggests that DRP retentions is approximately 13% of TP retention, reflecting the amount of DRP incorporated into algal biomass and removed from the water column by settling.

Load-response relationships – While it is common to assume that nutrient loads from different tributaries are mixed homogeneously in the receiving water body and contribute equally and proportionally to the load leaving the lake, our study illustrated that the spatial and temporal processing of individual loadings are important. Therefore, it is important to understand the "spatial-temporal variation" in the effects of tributary loads to help prioritize watersheds that can be most effective in per-unit load reductions.

The DRP response curve slopes (Fig. 4b) ranged from 0.53 to 0.65, indicating that the lake retains 35% to 47% of the tributary DRP loads, which is consistent with our model estimate of overall lake retention of 35% (base case; Table 6) and the slopes of the Thames and Sydenham rivers DRP response curves (Fig. 4b). A larger portion of the DRP load to Lake St. Clair comes from Lake Huron (St. Clair River; Table 3) in spring when phytoplankton biomass in Lake Huron is still small. For the tributaries with streamflow dominated by snowmelt and spring runoff (Thames and Sydenham rivers), a larger portion of DRP comes in spring. In spring, Lake St. Clair has a short water residence time, small phytoplankton biomass and insignificant DRP loss, so the DRP load leaves the lake very quickly (Bocaniov and Scavia, 2018). The Clinton river DRP retention is larger than for the overall lake retention and other two major tributaries (47% vs. 35%), because this river drains an urban area with a stable flow pattern and its DRP load of more equally distributed over the season including summer time when temperature, intensity of solar radiation and duration photoperiod, as well as higher phytoplankton biomass are all accelerating the DRP loss via phytoplankton uptake (Bocaniov and Scavia, 2018). A larger similarity between overall lake retention of DRP and those of the tributaries comes from the fact that DRP is a dissolved P and not affected by settling and resuspension processes as TP does.

The slopes of the TP (Fig. 4a) response curves ranged from 0.53 to 0.65, indicating tributary-specific retention rates of 47% to 35% compared to the overall lake retention rate of 17.3% (Table 5). This is likely because over 70% of the load to Lake St. Clair comes from the St. Clair River (Scavia et al., 2019) which has a WRT of 5 days, considerably smaller than those for the tributaries (8-11 days in spring; 21-39 days in summer and fall). The shorter residence time for St. Clair River water reduces the time available for biological processing of nutrients, reducing the potential for sedimentation and retention compared to the tributary waters.

Based on these export efficiencies, the Thames (0.64) is more efficient in reducing the TP load leaving the lake than the Sydenham (0.55) and the Clinton (0.54). For every 100 MT reduction in the load from the Thames, Sydenham, and Clinton, we would expect 64, 55, and 54 MT less leaving Lake St. Clair, respectively. Based on the DRP efficiencies, the Thames and Sydenham (0.65) are more efficient than the Clinton (0.53). The differences in slopes can be explained by the interactions of lake circulation and wind-induced resuspension, in the context of the seasonal timing of tributary loads.

Thames River water and P load is transported along the shallower south-east and east shore (Figs. 2 & 1b) where TP load that had settled to the lake bed can also be easily re-suspended and moved toward the lake's outflow. In addition, the Thames load is largest in late winter, early spring, and late fall (Fig. 6a-b), coinciding with variable and northeastern winds (Figs. SF–3c-d & SF–6c-d) and circulation pattern favoring flushing (Fig. SF–17d) and shorter river water residence times (~11 days). In late spring and summer, after most of the Thames P load has entered the lake, winds are westerly (e.g. Figs. SF–4a-d and SF–7a-d), with the strongest winds from the northwest driving circulation patterns (Fig. SF–17e-h) that increase Thames water residence times to 30 - 40 days.

While the Sydenham and Thames rivers hydrograph and DRP retention rates are similar, their TP retention rates differ. The Sydenham is located much further from the lake outflow and separated from it by a basin deep enough (≥ 5 m; Fig. 1a-b) to be net-depositional (e.g. Fig. 5d-f), thus enhancing particulate phosphorus retention resulting in a higher TP retention rate. The presence of the deep basin, however, would not affect DRP dynamics. Because both rivers have similar hydrographs and short residence times in spring (~11 days) when their DRP load is highest and phytoplankton growth is limited (Bocaniov and Scavia, 2018), DRP is quickly flushed from the lake resulting in similar load-response slopes.

Clinton River TP and DRP load-response curves have smaller slopes than the Thames, indicating larger portions of both are retained by the lake. The Clinton River load is more evenly distributed over the seasons (Fig. 6a-b), therefore a substantial amount of it is delivered during periods of higher production and settling, leading to higher nutrient retention rates. The Clinton River water mass also mixes over a larger area, allowing TP settling not only in the naturally deeper parts of the lake but also the deeper, ~8.4 m navigational channel (Fig. 1b). The load can also be advected to a small bay in the north (Anchor Bay) or to the L'anse Creuse Bay (Figs. 3 &1a) and be trapped there.

While tributary load reductions will result in reduced load leaving the lake, those reductions are likely to be small compared to the overall load. For example, because the average baseline load leaving Lake St. Clair during the simulation was 1597 MT, even 50% reductions in tributary loads will reduce the load leaving the lake by less than 5%. However, it is important to explore their differences because they will likely receive management attention, particularly for controlling non-point sources.

Conclusions and Implications for Lake Erie load reduction

Based on our results for this large, shallow lake, Lake St. Clair is a net sink for nutrients and this attenuation capacity can modify the magnitude and seasonal dynamics of nutrient loads. Contrary to the general assumption that tributary inflows and nutrient loads in large shallow polymictic (vertically well-mixed) systems are mixed homogeneously and equally and proportionally exported to the lake's outflow and further downstream, we showed that spatial and temporal variation in tributary loads are important. The fact that the lake retains 35% of its DRP input (this study) and, on average, 20% of its TP load (Scavia et al., 2019), that the retention rates are highly dependent on winds (this study), and that there are differences in the retention rates for different tributaries are important considerations when allocating load reductions to Lake Erie.

There are many shallow water bodies around the world similar to Lake St. Clair and showing signs of ongoing or accelerated eutrophication where our findings may be applied. Examples of such systems include, but not limited to, large shallow lakes (e.g. Lake Winnipeg, Lake Manitoba, western basin of Lake Erie) and numerous smaller lakes and reservoirs, including many shallow and productive lakes and reservoirs that are imbedded within larger watersheds and similarly process nutrients between upper and lower reaches.

Acknowledgements

This work was funded by the Fred A and Barbara M Erb Family Foundation grant number 903, the University of Michigan's Graham Sustainability Institute, and the University of Waterloo's Lake Futures and Global Water Futures Project. We appreciate the help, insights and

advice offered by the University of Michigan's Dave Schwab, Lynn Vaccaro, Awoke Dagnew, Colleen Long, Yu-Chen Wang, and Jennifer Read. We appreciate the data graciously provided by Debbie Burniston, Alice Dove, Sean Backus, Luis Leon, Mohamed Mohamed, and Reza Valipour from Environment and Climate Change Canada, and Katie Stammler from the Essex Region Conservation Authority. Data related to this article can be found at the Polar Data Catalogue (PDC) website (https://tinyurl.com/y2hst526).

References

Anderson, E. J., & Schwab, D. J. (2011). Relationships between wind-driven and hydraulic flow in Lake St. Clair and the St. Clair River Delta. *Journal of Great Lakes Research*, 37(1), 147-158.

Anderson, E. J., Schwab, D. J., & Lang, G. A. (2010). Real-time hydraulic and hydrodynamic model of the St. Clair River, Lake St. Clair, Detroit River system. *Journal of Hydraulic Engineering*, 136(8), 507-518.

Bocaniov, S. A., & Scavia, D. (2018). Nutrient loss rates in relation to transport time scales in a large shallow lake (Lake St. Clair, USA – Canada): insights from a three-dimensional lake model. *Water Resources Research*, 54, 3825-3840.

Bocaniov, S. A., & Scavia, D. (2016). Temporal and spatial dynamics of large lake hypoxia: Integrating statistical and three-dimensional dynamic models to enhance lake management criteria. *Water Resources Research*, 52, 4247-4263.

Bocaniov, S. A., Leon, L. F., Rao, Y. R., Schwab, D. J., & Scavia, D. (2016). Simulating the effect of nutrient reduction on hypoxia in a large lake (Lake Erie, USA-Canada) with a three-dimensional lake model. *Journal of Great Lakes Research*, 42 (6), 1228–1240.

Bocaniov, S. A., Ullmann, C., Rinke, K., Lamb, K. G., & Boehrer, B. (2014a). Internal waves and mixing in a stratified reservoir: Insights from three-dimensional modeling. *Limnologica -Ecology and Management of Inland Waters*, 49, 52-67.

Bocaniov, S. A., Smith, R. E., Spillman, C. M., Hipsey, M. R., & Leon, L. F. (2014b). The nearshore shunt and the decline of the phytoplankton spring bloom in the Laurentian Great Lakes: insights from a three-dimensional lake model. *Hydrobiologia*, 731(1), 151-172.

Bridgeman, T. B., Chaffin, J. D., & Filbrun, J. E. (2013). A novel method for tracking western Lake Erie Microcystis blooms, 2002–2011. *Journal of Great Lakes Research*, 39, 83–89.

Burniston, D., Dove, A., Backus, S., & Thompson, A. (2018). Nutrient concentrations and loadings in the St. Clair River–Detroit River Great Lakes interconnecting channel. *Journal of Great Lakes Research*, 44, 398-411.

Charlton, M. N., Milne, J. E., Booth, W. G., & Chiocchio, F. (1993). Lake Erie offshore in 1990: restoration and resilience in the central basin. *Journal of Great Lakes Research*, 19(2), 291-309.

GLWQA (Great Lakes Water Quality Agreement) (2016). The United States and Canada adopt phosphorus load reduction targets to combat Lake Erie algal blooms, https://tinyurl.com/y4y8nsm3 (assessed February 25, 2018).

Dagnew, A., Scavia, D., Wang, Y.C., Muenich, R., & Kalcic, M. (2019). Modeling phosphorus reduction strategies from the international St. Clair-Detroit River system watershed. *Journal of Great Lakes Research* (https://doi.org/10.1016/j.jglr.2019.04.005).

Dean, R. G., & Dalrymple, R. A. (1984). *Water wave mechanics for engineers and scientists*. Prentice Hall, Inc., Englewood Cliffs, New Jersey, ISBN 0-13-946038-1.

Glenn, S. M., & Grant, W. D. (1987). A suspended sediment stratification correction for combined wave and current flows. *Journal of Geophysical Research: Oceans*, 92(C8), 8244–8264.

Grant, W.D., & Madsen, O. S. (1979). Combined wave and current interaction with a rough bottom. *Journal of Geophysical Research: Oceans*, 84(C4), 1797–1808.

Hamilton, D. P., & Mitchell, S. F. (1996). An empirical model for sediment resuspension in shallow lakes. *Hydrobiologia*, 317/3, 209–220.

636 Hamilton, D., & Mitchell, S. (1997). Wave-induced shear stresses, plant nutrients and
637 chlorophyll in seven shallow lakes. *Freshwater biology*, 38(1), 159-168.
638 Hawley, N., & Lesht, B. M. (1992). Sediment resuspension in Lake St. Clair. *Limnology and*
639 *oceanography*, 37(8), 1720-1737.
640 Hipsey, M. R., & Hamilton, D. P. (2008). Computational Aquatic Ecosystem Dynamics Model:
641 CAEDYM v3. v3.3 Science Manual (DRAFT). Centre for Water Research (CWR),
642 University of Western Australia.
643 Ho, J. C., & Michalak, A. M. (2015). Challenges in tracking harmful algal blooms: A synthesis
644 of evidence from Lake Erie. *Journal of Great Lakes Research*, 41(2), 317-325.
645 Hipsey, M. R. (2008). The CWR computational aquatic ecosystem dynamics model CAEDYM.
646 User Manual. Centre for Water Research (CWR), University of Western Australia.
647 Hu, Y., Scavia, D., & Kerkez, B. (2018). Are all data useful? Inferring causality to predict flows
648 across sewer and drainage systems using Directed Information and Boosted
649 Regression Trees. *Water Resources*, 145, 697-706.
650 HYDAT (2018). Canada's HYDAT National Water Data Archive, http://tinyurl.com/y8be92pz
651 (assessed February 1, 2018).
652 IJC (International Joint Commission) (1978). Great Lakes Water Quality Agreement of 1978,
653 with annexes and terms of reference, between the United States of America and Canada.
654 IJC: Windsor, Ontario, Canada, November 22, 1978.
655 IJC (International Joint Commission) (2012). Great Lakes Water Quality Agreement 2012.
656 Protocol amending the agreement between Canada and the United States of America on
657 Great Lakes water quality. IJC: Windsor, Ontario, Canada, September 7, 2012.

IJC (International Joint Commission) (2017). Draft domestic action plans for achieving phosphorus reductions in Lake Erie. Available at Canada-United States collaboration for Great Lakes water quality website: https://binational.net/2017/03/10/dap-pan/

Karatayev, A. Y., Burlakova, L. E., Mehler, K., Bocaniov, S. A., Collingsworth, P. D., Warren, G., Kraus, R. T., & Hinchey, E. K. (2018). Biomonitoring using invasive species in a large lake: Dreissena distribution maps hypoxic zones. *Journal ofGreat Lakes Research*, 44(4), 639-649.

Kalcic, M. M., Kirchhoff, C., Bosch, N., Muenich, R. L., Murray, M., Griffith Gardner, J., & Scavia, D. (2016). Engaging stakeholders to define feasible and desirable agricultural conservation in western Lake Erie watersheds. *Environmental Science & Technology*, 50(15), 8135-8145.

Kestin, J., Sokolov, M., & Wakeham, W. A. (1978). Viscosity of liquid water in the range − 8 C to 150 C. *Journal of Physical and Chemical Reference Data*, 7(3), 941-948.

Lang, G. A., Morton, J. A., & Fontaine III, T. D. (1988). Total phosphorus budget for Lake St. Clair: 1975–80. *Journal of Great Lakes Research*, 14(3), 257-266.

Leon, L. F., Smith, R. E., Hipsey, M. R., Bocaniov, S. A., Higgins, S. N., Hecky, R. E., Antenucci, J. P., Imberger, J. A., & Guildford, S. J. (2011). Application of a 3D hydrodynamic–biological model for seasonal and spatial dynamics of water quality and phytoplankton in Lake Erie. *Journal of Great Lakes Research*, 37(1), 41-53.

Liu, W., Bocaniov, S. A., Lamb, K. G., & Smith, R. E., 2014. Three dimensional modeling of the effects of changes in meteorological forcing on the thermal structure of Lake Erie. *Journal of Great Lakes Research*, 40(4), 827-840.

Ludsin, S. A., Kershner, M. W., Blocksom, K. A., Knight, R. L., & Stein, R. A. (2001). Life after death in Lake Erie: nutrient controls drive fish species richness, rehabilitation. *Ecological Applications*, 11(3), 731-746.

Luettich Jr, R. A., Harleman, D. R., & Somlyody, L. (1990). Dynamic behavior of suspended sediment concentrations in a shallow lake perturbed by episodic wind events. *Limnology and Oceanography*, 35(5), 1050–1067.

Maccoux, M. J., Dove, A., Backus, S. M., & Dolan, D. M. (2016). Total and soluble reactive phosphorus loadings to Lake Erie: A detailed accounting by year, basin, country, and tributary. *Journal of Great Lakes Research*, 42, 1151-1165.

Masselink, G., Hughes, M., & Knight, J. (2014). *Introduction to Coastal Processes and Geomorphology*. Routledge.

Michalak, A. M., Anderson, E. J., Beletsky, D., Boland, S., Bosch, N. S., Bridgeman, T. B., Chaffin, J. D., Cho, K., Confesor, R., Daloğlu, I., & DePinto, J. V. (2013). Record-setting algal bloom in Lake Erie caused by agricultural and meteorological trends consistent with expected future conditions. *Proceedings of the National Academy of Sciences*, 110(16), 6448-6452.

Muenich, R. L., Kalcic, M., & Scavia, D. (2016). Evaluating the impact of legacy P and agricultural conservation practices on nutrient loads from the Maumee River watershed. *Environmental Science & Technology*, 50(15), 8146-8154.

Nalepa, T. F., Gardner, W.S., & Malczyk, J. M. (1991). Phosphorus cycling by mussels (Unionidae: Bivalvia) in Lake St. Clair. *Hydrobiologia*, 219(1), 239-250.

Nalepa, T. F., Hartson, D.J., Gostenik, G. W., Fanslow, D. L., & Lang, G. A. (1996). Changes in the freshwater mussel community of Lake St. Clair: from Unionidae to Dreissena polymorpha in eight years. *Journal of Great Lakes Research*, 22(2), 354-369.

Oveisy, A., Rao, Y. R., Leon, L. F., & Bocaniov, S. A. (2014). Three-dimensional winter modeling and the effects of ice cover on hydrodynamics, thermal structure and water quality in Lake Erie. *Journal of Great Lakes Research*, 40, 19-28.

Scavia, D., Allan, J. D., Arend, K. K., Bartell, S., Beletsky, D., Bosch, N. S., Brandt, S. B., Briland, R. D., Daloğlu, I., DePinto, J. V., Dolan, D. M., Evans, M. A., Farmer, T. M., Goto, D., Han, H., Höök, T. O., Knight, R., Ludsin, S. A., Mason, D., Michalak, A. M., Richards, R. P., Roberts, J. J., Rucinski, D. K., Rutherford, E., Schwab, D. J., Sesterhenn, T., Zhang, H., & Zhou, Y. (2014) Assessing and addressing the re-eutrophication of Lake Erie: Central basin hypoxia. *Journal of Great Lakes Research*, 40(2), 226-246.

Scavia, D., DePinto, J. V., & Bertani, I. (2016). A Multi-model approach to evaluating target phosphorus loads for Lake Erie. *Journal of Great Lakes Research*, 42, 1139-1150.

Scavia, D., Kalcic, M., Muenich, R. L., Read, J., Aloysius, N., Bertani, I., Boles, C., Confesor, R., DePinto, J., Gildow, M., & Martin, J. (2017). Multiple models guide strategies for agricultural nutrient reductions. *Frontiers in Ecology and the Environment*, 15(3), 126-132.

Scavia, D., Bocaniov, S. A., Dagnew, A., Long, C. M., & Wang, Y.-C. (2019). St. Clair - Detroit River system: Phosphorus mass balance and implications for Lake Erie load reduction, monitoring, and climate change. *Journal of Great Lakes Research*, 45, 40-49.

Schwab, D. J., Clites, A. H., Murthy, C. R., Sandall, J. E., Meadows, L.A., & Meadows, G. A., 1989. The effect of wind on transport and circulation in Lake St. Clair. *Journal of Geophysical Research*: *Oceans*, 94(C4), 4947-4958.

724 Tanaka, M., Girard, G., Davis, R., Peuto, A., & Bignell, N. (2001). Recommended table for the
725 density of water between 0 C and 40 C based on recent experimental reports. *Metrologia*,
726 38(4), 301-309.
727 Tsai, C. H., & Lick, W. (1986). A portable device for measuring sediment resuspension. *Journal*
728 *of Great Lakes Research*, 12(4), 314-321.
729 U.S. Geological Survey (2018). U.S. Geological Survey National Water Information System -
730 Web Interface (2018), https://waterdata.usgs.gov/nwis (accessed February 18, 2018).
731 Van Rijn, L. C. (1993). *Principles of sediment transport in rivers, estuaries and coastal*
732 *seas* (Vol. 1006). Amsterdam: Aqua publications.
733 Zhou, Y., Michalak, A. M., Beletsky, D., Rao, Y. R., & Richards, R. P. (2015). Record-breaking
734 Lake Erie hypoxia during 2012 drought. *Environmental Science & Technology*, 49(2), 800-
735 807.

Figures Legends:

Figure 1. (a) Map of Lake St. Clair with the lake outflow, Detroit River, and 17 included tributaries indicated by arrows with numbers corresponding to their names in Table 3. Open triangles indicate the locations of in-lake buoy (#45147) and water level gauging stations, while solid circles show the deployment locations of instrumented tripods in 2016 (stations A1-2); (b) Bathymetric map of Lake St. Clair. The deep channel dissecting lake from north to southwest is the navigational channel.

Figure 2. Maps showing spatial and temporal distribution of the Thames River water at the lake surface (depth: 0.2 m) expressed as a percent of the original Thames River water (monthly-averaged value).

Figure 3. Maps showing spatial and temporal distribution of the Clinton River water at the lake surface (depth: 0.2 m) expressed as a percent of the original Clinton River water (monthly-averaged value).

Figure 4. Lake St. Clair (LSC) outflow response curves for three major tributaries: (a) for total phosphorus - TP; and, (b) for dissolved reactive phosphorus - DRP. Please note that the regression intercepts were subtracted from the full load leaving Lake St. Clair (y-axis).

Figure 5. Wave-induced hourly bottom shear stress (τ_w; N m^{-2}) calculated for the lake bottom at different depths: (a) 2 m; (b) 3 m; (c) 4 m; (d) 5 m; (e) 6 m; and, (f) 6.4 m. The data used in calculations (significant wave height and wave period) are based on hourly observations in 2009 at the in-lake buoy # 45147 (Fig. 1a). Open circles and darker shaded area indicate percent of daily lake ice cover in 2009, while lighter shaded area indicate values of hourly bottom shear stress which are below the critical value (τ_{crit}) of 0.25 N m^{-2} (Tsai and Lick, 1986). PTA indicates the percent of the entire time when $\tau_w > \tau_{crit}$.

Figure 6. (a) Mean monthly discharges averaged from 2000 to 2017 for the St. Clair River (yellow squares) and three major tributaries: Thames (blue circles), Sydenham (brown triangles), and

761 Clinton (black diamonds) rivers; (b) Mean monthly discharge as a proportion of total annual
762 discharge over the period 2000 through 2017 for the same rivers as in (a); (c) Lake St. Clair water
763 age in May and August 2009 estimated by Bocaniov and Scavia (2018).

Table 1. Long term (1918 - 2017) monthly mean water levels for Lake St. Clair (meters; IGLD85*) and corresponding mean lake water volumes (km^3), mean and maximum depths (m)**.

Month	Mean Value
Jan	174.84
Feb	174.79
Mar	174.90
Apr	175.04
May	175.13
Jun	175.18
Jul	175.20
Aug	175.16
Sept	175.09
Oct	175.00
Nov	174.91
Dec	174.91
Mean Water Level* (m):	175.01
Mean Volume** (km^3):	4.3
Mean Depth** (m):	3.9
Max Depth** (m):	6.4

* All levels are referenced to the International Great Lakes Datum of 1985 (IGLD 85).
** Calculations were based on the bathymetric map of Lake St. Clair and water level measurements at the three water level gauging stations (Table ST-1; Fig. 1a): #9034052, # 9044049, and #11965.

Table 2. Characterization of the sub-watersheds within St. Clair River – Lake St. Clair (SCR-LSC) system.

#	System Component	Watershed Area (km^2)			As % of the entire SCR -LSC system
		USA	Canada	Total	
1	St. Clair River*	2,997	502	3,499	22.7
2	Lake St. Clair, including:	2,727	9,181	11,908	77.3
2.1	Clinton River	2,064	-	2,064	13.4
2.2	Thames River	-	5,875	5,875	38.1
2.3	Sydenham River	-	2,676	2,676	17.4
2.4	other tributaries	663	630	1,293	8.4
	Total	5,724	9,683	15,407	100
	As % of the SCR – LSC system	37.2	62.8	100	

* the upstream watershed of the St. Clair River arising from the drainage of the upper Laurentian Great Lakes (Lakes Superior, Michigan and Huron) is 576,014 km^2 and not included in the table.

Table 3. Average flows and total loading (March 1 to October 31 inclusive) of total phosphorus (TP) and dissolved reactive phosphorus (DRP) in metric tonnes (MT) for various tributaries to Lake St. Clair for the base case scenario (Table 4).

#	Tributary Name	Total TP Load (MT)	Total DRP Load (MT)	Daily Flow ($m^3 s^{-1}$)	As % of Total Lake Input		
					TP (%)	DRP (%)	Tributary inflow (%)
1	St. Clair River	1507.873	448.551	5384.696	78.13	71.88	97.762
2	Thames River	200.873	70.835	68.412	10.41	11.35	1.242
3	Sydenham River	72.785	27.799	28.418	3.77	4.45	0.516
4	Clinton River	89.520	48.224	19.393	4.64	7.73	0.352
5	Ruscom River	3.603	2.018	0.818	0.19	0.32	0.015
6	Belle River	2.368	1.326	0.538	0.12	0.21	0.010
7	Pike Creek	2.024	1.134	0.460	0.10	0.18	0.008
8	Salt River	5.570	4.568	1.385	0.29	0.73	0.025
9	Puce River	1.559	0.873	0.354	0.08	0.14	0.006
10	Little River	2.475	1.386	0.562	0.13	0.22	0.010
11	Swan Creek	1.318	1.028	1.021	0.07	0.16	0.019
12	Beauben Creek	2.528	2.199	0.796	0.13	0.35	0.014
13	Little Ceek	1.397	0.782	0.317	0.07	0.13	0.006
14	Moison Creek	0.515	0.288	0.117	0.03	0.05	0.002
15	Marsac Creek	0.844	0.692	0.318	0.04	0.11	0.006
16	Duck Creek	0.441	0.247	0.100	0.02	0.04	0.002
17	Crapaud Creek	0.786	0.645	0.296	0.04	0.10	0.005
	Atmospheric load	33.428	11.430	36.983	1.73	1.83	0.671
	Total:	1929.907	624.025				

Table 4. Meteorological forcing scenarios represented by the base case scenario (scenario B) and eight additional scenarios (C1 to C8) using the same initial, boundary and forcing (inflow-outflow) conditions as in case B except for the meteorological forcing indicative of those observed during a particular year.

Scenario #	Meteorological forcing conditions (year)	Scenario details and modifications made relative to the base case scenario (Scenario B):
Base case (B)	2009	Base case scenario B (model calibrated for 2009)
C1	1995	Different meteorological conditions indicative of 1995
C2	1996	Different meteorological conditions indicative of 1996
C3	2003	Different meteorological conditions indicative of 2003
C4	2005	Different meteorological conditions indicative of 2005
C5	2008	Different meteorological conditions indicative of 2008
C6	2010	Different meteorological conditions indicative of 2010
C7	2012	Different meteorological conditions indicative of 2012
C8	2014	Different meteorological conditions indicative of 2014

Table 5. Retention of total phosphorus (R_{TP}) from March 1 to October 31 inclusive under different meteorological forcing scenarios. Retention is determined as the difference between TP entering and leaving the lake (TP_IN and TP_OUT). MT means metric tonnes.

Scenario	Season average air temperature	Season average wind speed	Total Phosphorus (TP)			
	$\overline{AT}$ (°C)	$\overline{WS}$ (m s^{-1})	TP_IN (MT)	TP_OUT (MT)	R_{TP} (MT)	R_{TP} (%)
Base case (B)	15.37	6.02	1929.907	1596.9	333.01	17.26
C1	15.71	6.44	1929.907	1632.7	297.21	15.40
C2	14.72	6.59	1929.907	1672.9	257.01	13.32
C3	14.80	6.03	1929.907	1585.1	344.81	17.87
C4	16.74	5.82	1929.907	1530.0	399.91	20.72
C5	15.72	5.91	1929.907	1550.6	379.31	19.65
C6	17.20	6.04	1929.907	1567.1	362.81	18.80
C7	17.41	6.09	1929.907	1563.7	366.21	18.98
C8	15.19	6.12	1929.907	1608.2	321.71	16.67
				Average:	340.22	17.63

Table 6. Retention of total dissolved phosphorus (R_{DRP}) from March 1 to October 31 inclusive under different meteorological forcing scenarios. Retention is determined as the difference between amount of DRP entering and leaving the lake (DRP_IN and DRP_OUT). MT means metric tonnes.

Scenario	Season average air temperature	Season average wind speed	Dissolved Reactive Phosphorus (DRP)			
	$\overline{AT}$ (°C)	$\overline{WS}$ (m s^{-1})	DRP_IN (MT)	DRP_OUT (MT)	R_{DRP} (MT)	R_{DRP} (%)
Base case (B)	15.37	6.02	624.025	406.9	217.125	34.79
C1	15.71	6.44	624.025	410.2	213.825	34.27
C2	14.72	6.59	624.025	423.0	201.025	32.21
C3	14.80	6.03	624.025	409.6	214.425	34.36
C4	16.74	5.82	624.025	397.0	227.025	36.38
C5	15.72	5.91	624.025	407.4	216.625	34.71
C6	17.20	6.04	624.025	404.0	220.025	35.26
C7	17.41	6.09	624.025	403.2	220.825	35.39
C8	15.19	6.12	624.025	398.7	225.325	36.11
				Average:	217.358	34.83

Table 7. Simple and multiple ordinary least squared (OLS) regression models relating retention of total phosphorus (R_{TP}; MT) and dissolved reactive phosphorus (R_{DRP}; MT) to explanatory variables such as season averaged values of air temperature ($\overline{AT}$; $°C$) and wind speed ($\overline{WS}$; m s^{-1}) for simulation scenarios listed in Table 4 (N = 9).

Model	Dependent variable	Regression	R^2	P-value
1	R_{TP}	(1370.08** ±140.74) - (168.34** ±22.99)·[$\overline{WS}$]	0.885	<0.001
2	R_{TP}	(-109.09 ±199.54) + (28.31 ±12.55)·[$\overline{AT}$]	0.421	0.059
3	R_{TP}	(1013.63** ±129.96) - (145.16** ±15.29)·[$\overline{WS}$] + (13.52* ±3.73)·[$\overline{AT}$]	0.964	<0.001
4	R_{DRP}	(364.15** ±45.49) – (23.99* ±7.43)·[$\overline{WS}$]	0.601	0.014
5	R_{DRP}	(149.78** ±37.56) + (4.26 ±2.37)·[$\overline{AT}$]	0.317	0.114
6	R_{DRP}	(306.23** ±68.24) – (20.23* ±8.03)·[$\overline{WS}$] + (2.20 ±1.96)·[$\overline{AT}$]	0.668	0.037
7	R_{DRP}	(172.25** ±14.46) + (0.13* ±0.04)·[R_{TP}]	0.585	0.016

* significant at the $0.01 < P \leq 0.05$ level; ** significant at the $P < 0.01$ level; ± standard errors of the regression parameters; R^2, coefficient of determination; N, number of observations; for the multiple regressions, the independent variables are listed in a decreasing order of explained variance; MT, metric tonnes.

43 Table 8. The allocation of lake bottom areas for various depth zones in Lake St. Clair.

Depth range (meters)	Bottom Area (km^2)	As % of total lake bottom (%)
0 – 0.9	102	9.2
1 – 1.9	170	15.3
2 – 2.9	90	8.1
3 – 3.9	179	16.1
4 – 4.9	246	22.1
5 – 5.9	287	25.8
6 – 6.4	40	3.6
Total:	1114	100

44

Figure 1.

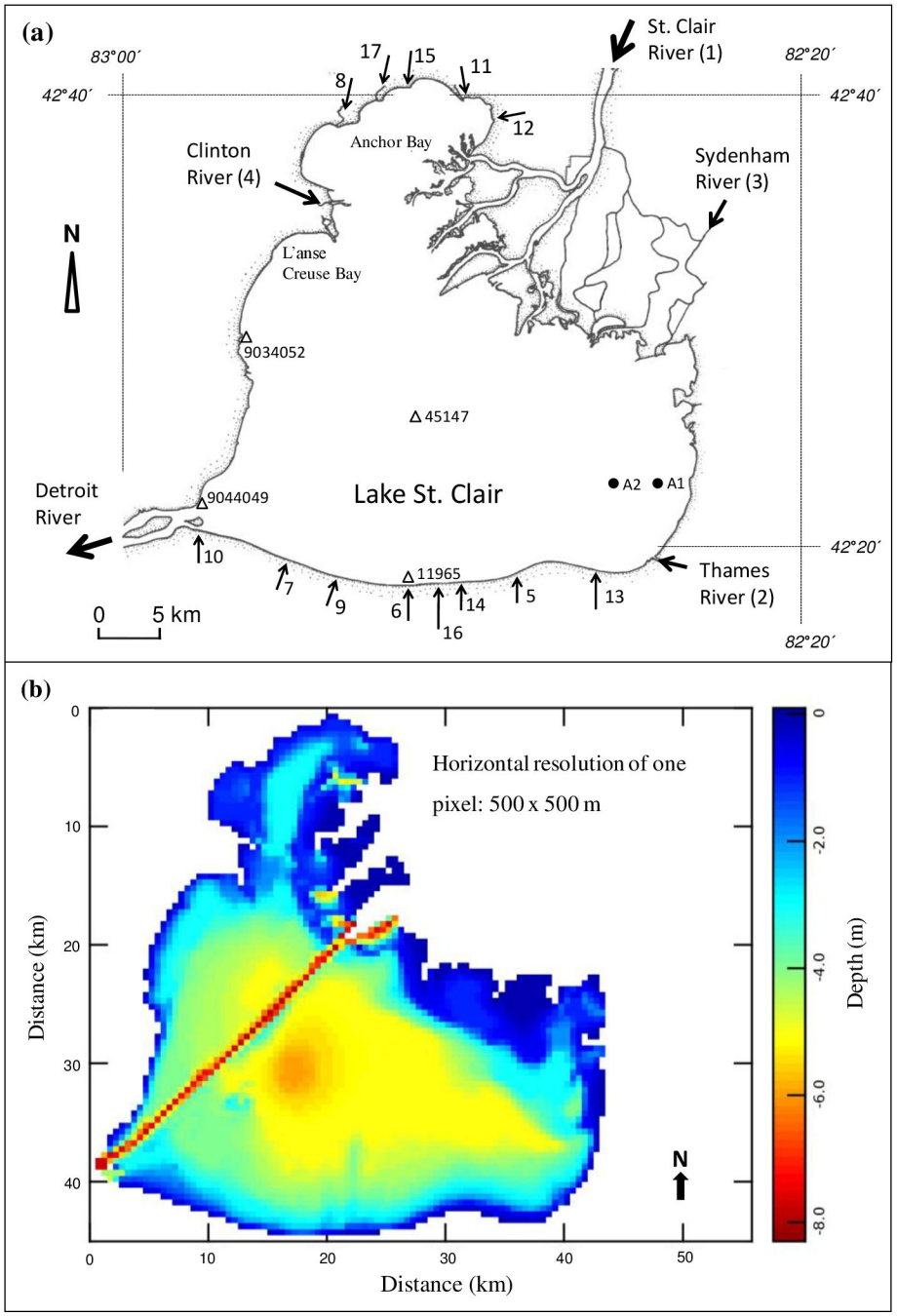

Figure 2.

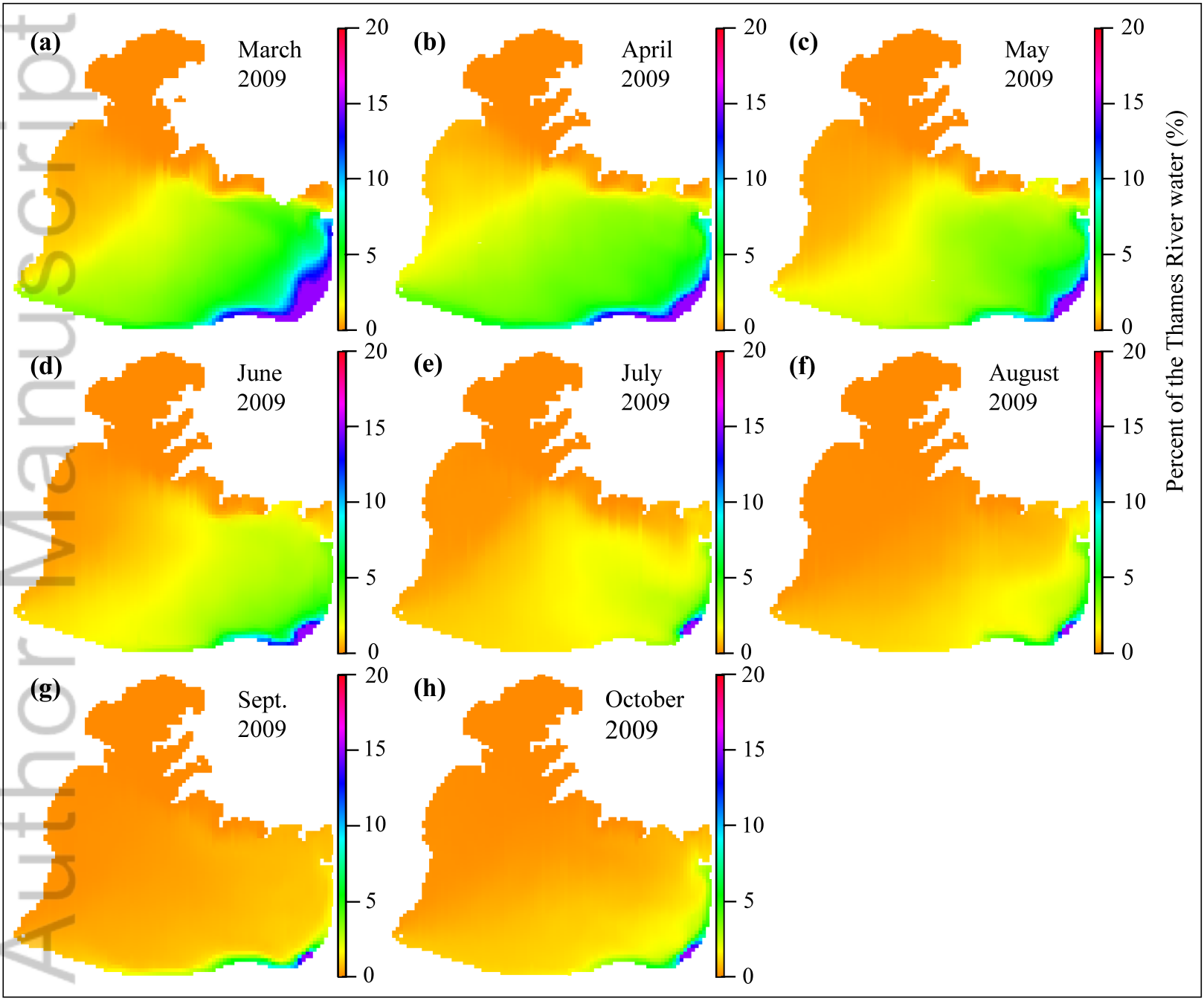

Figure 3.

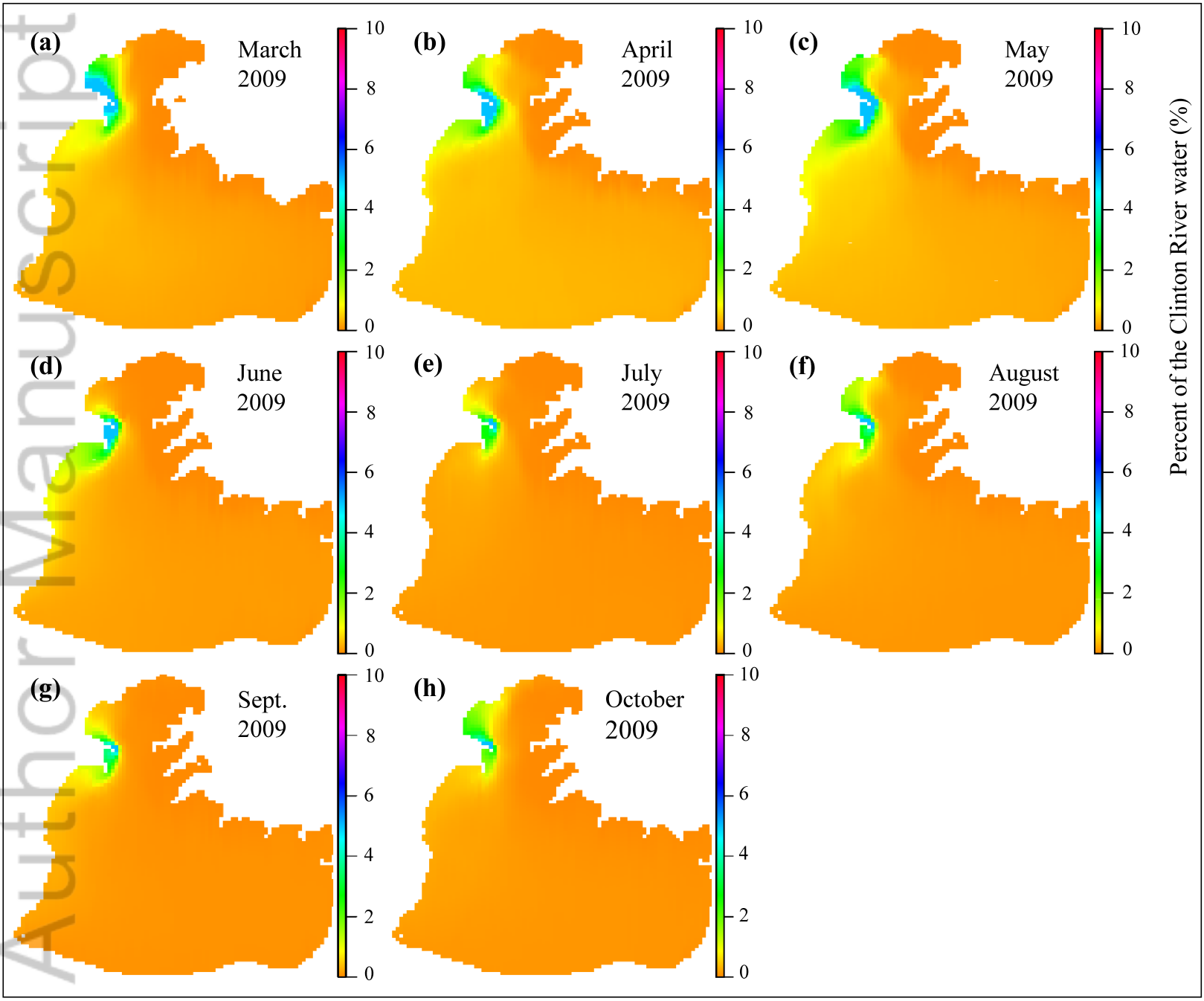

Figure 4.

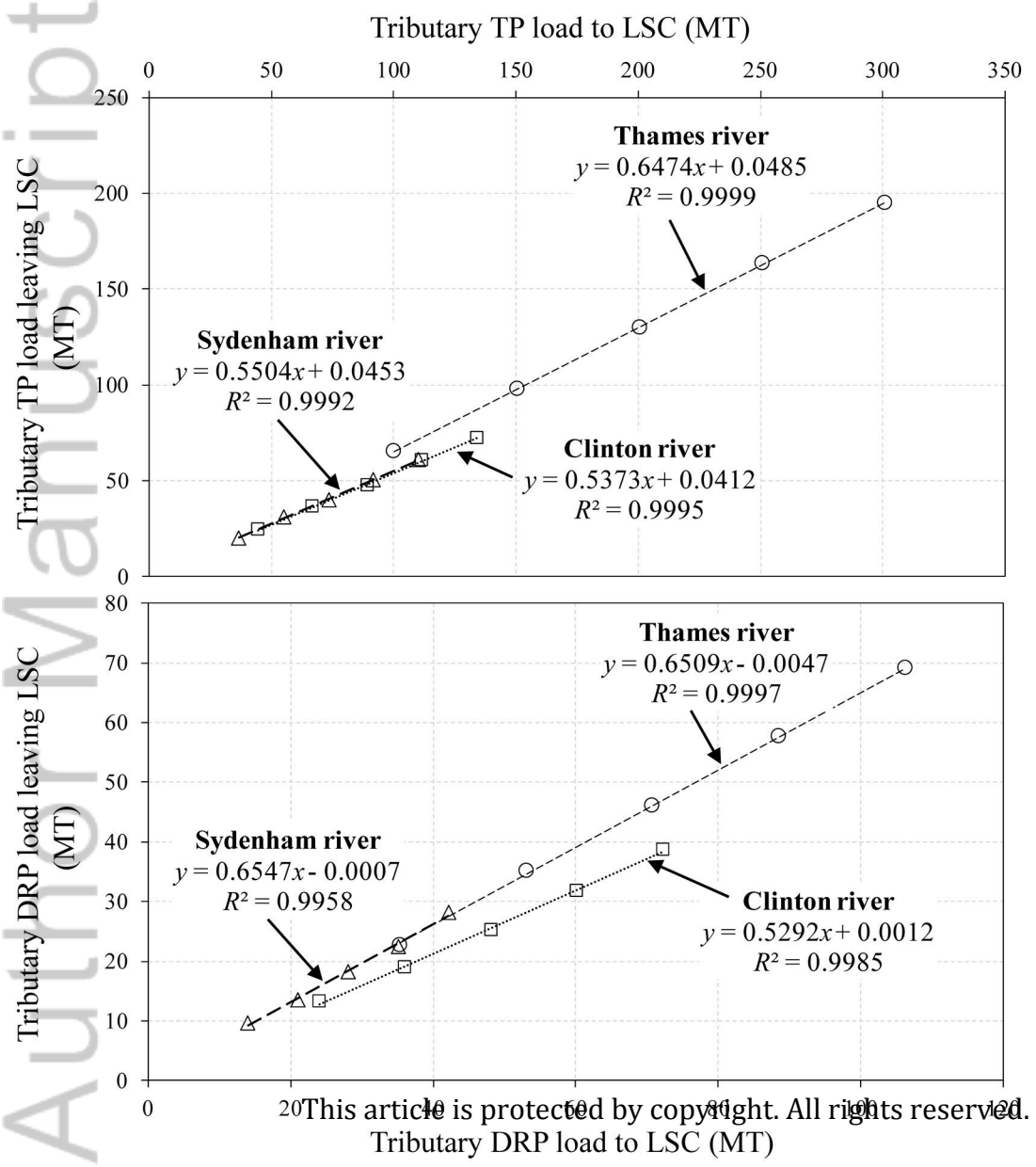

Figure 5.

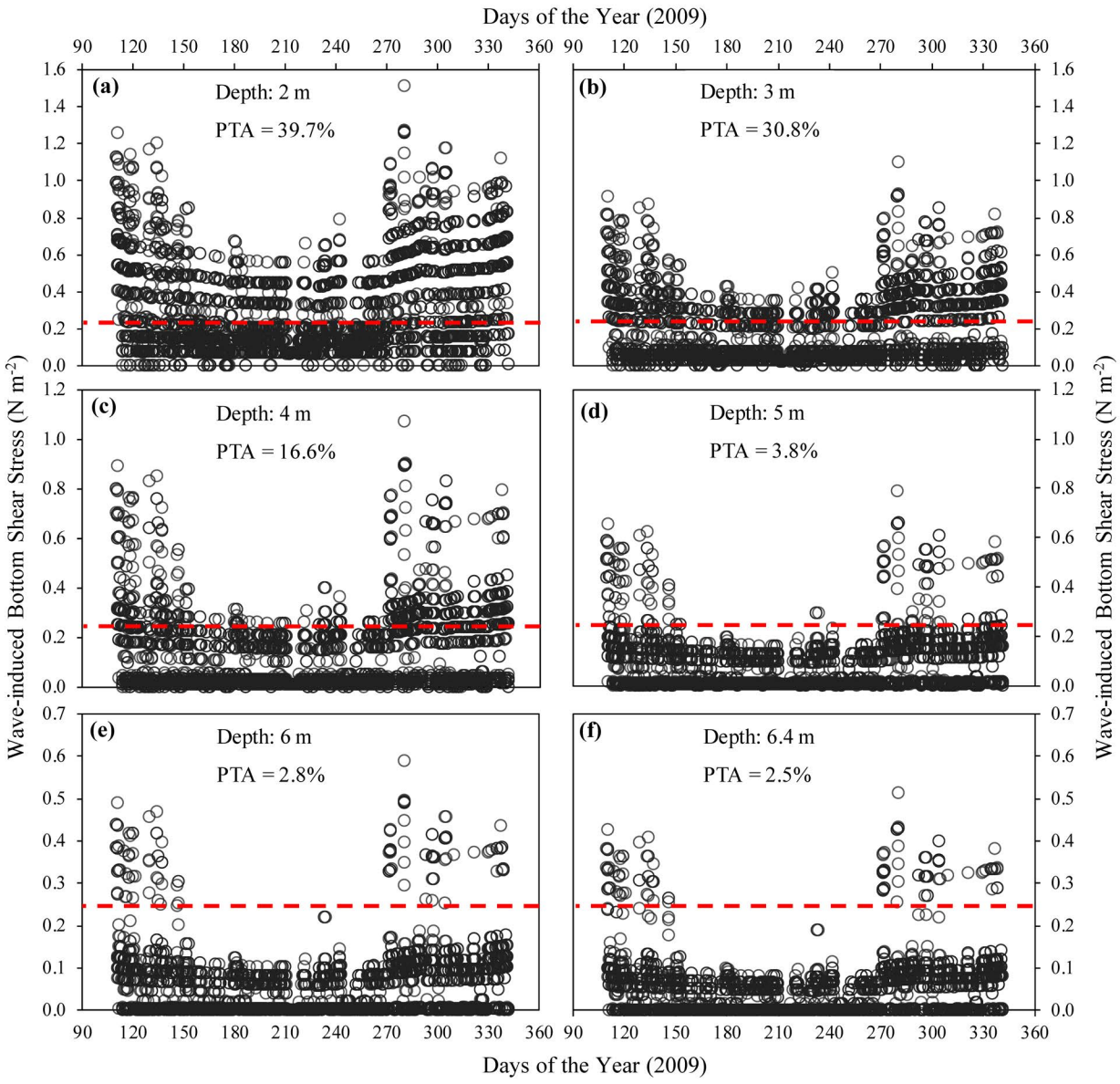

Figure 6.

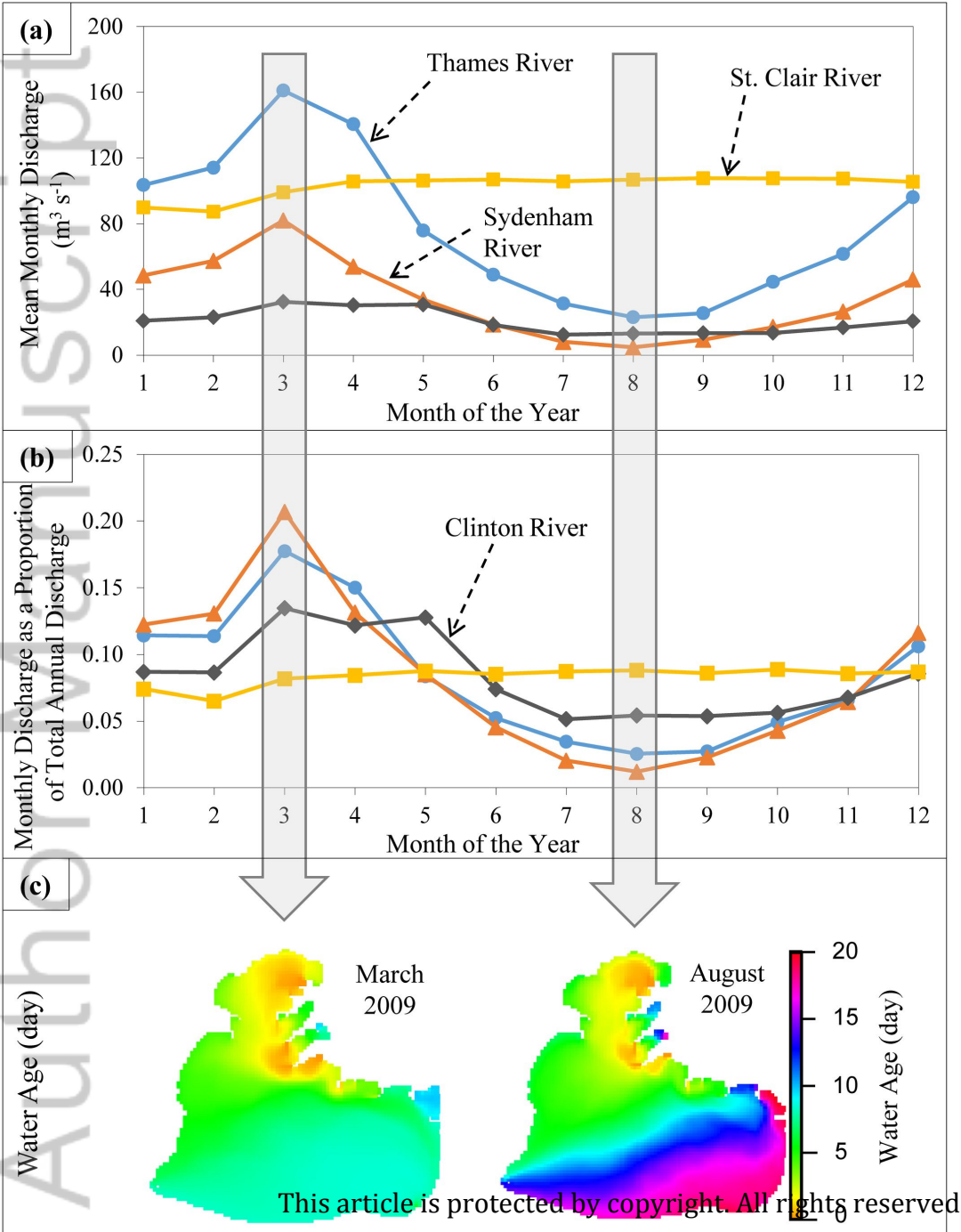

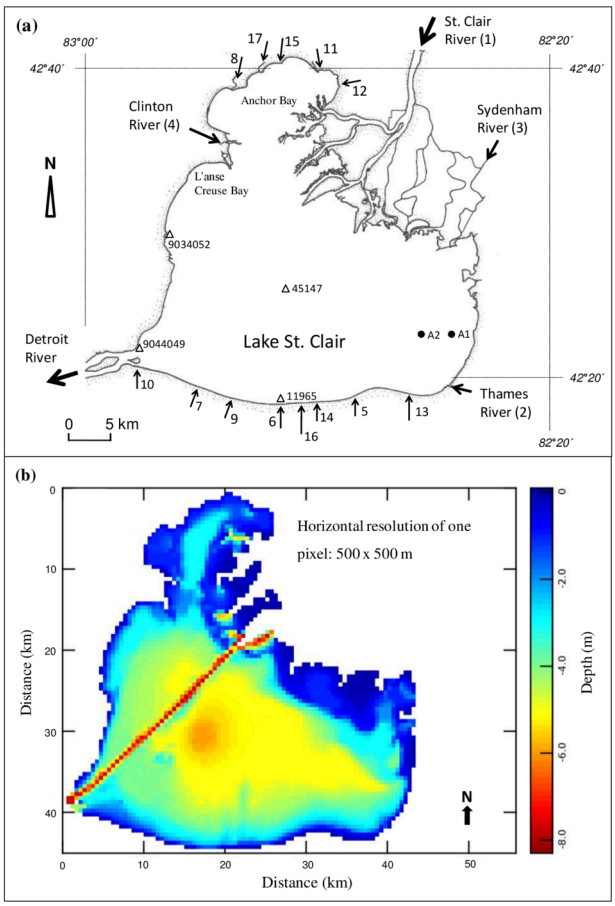

2019WR025019-f01-z-.tif

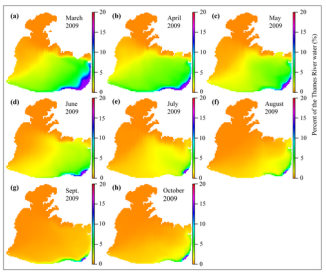

2019WR025019-f02-z-.tif

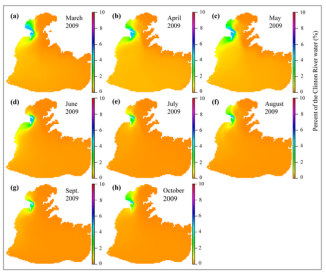

2019WR025019-f03-z-.tif

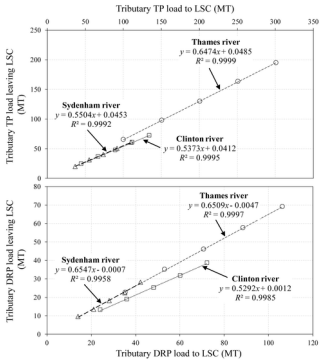

2019WR025019-f04-z-.tif

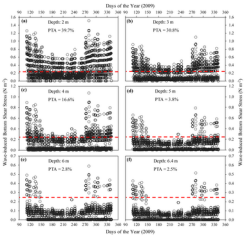

2019WR025019-f05-z-.tif

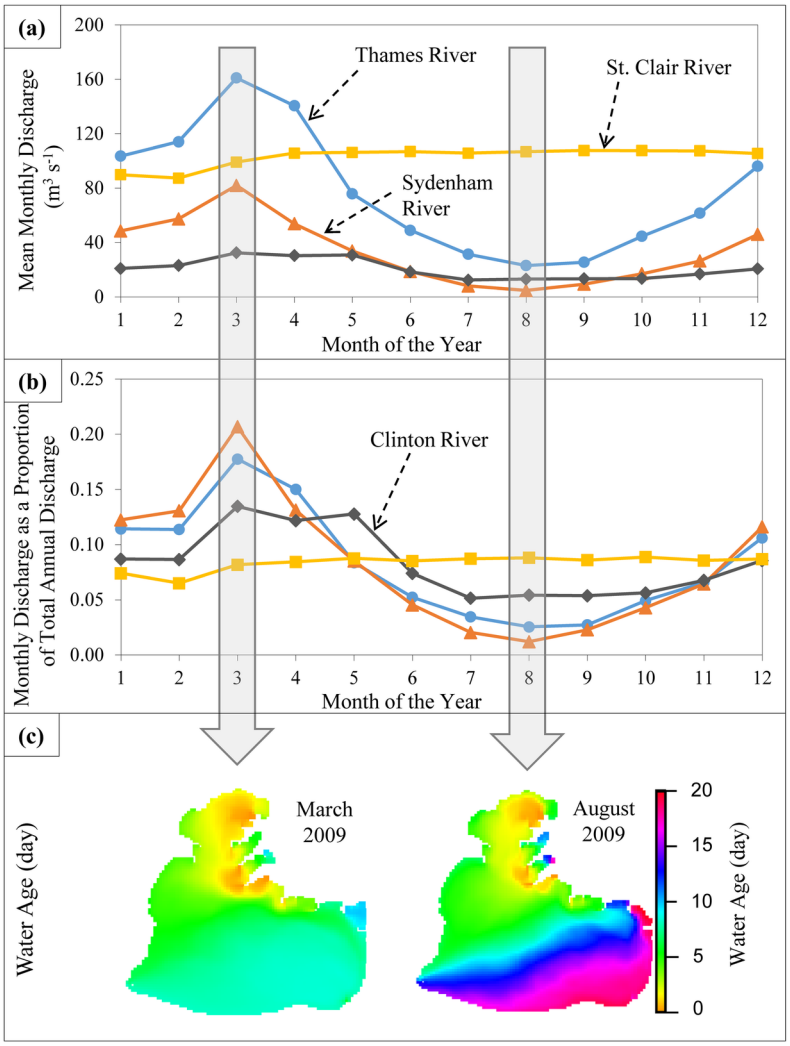

2019WR025019-f06-z-.png